IOSR Journal of Engineering (IOSRJEN) **www.iosrjen.org**
ISSN (e): 2250-3021, ISSN (p): 2278-8719
Vol. 10, Issue 4, April 2020, ||Series -I|| PP 44-57

Potent antifungal activity ofZnONanoparticles on *R.mucilaginosa*is mediated by reactive oxygen species and zinc ion

Ho Jinn Shyuan[aξ], Aziz AzzahraaIzzati[aξ], Pung YuhFen[a]*, Chew Hui Yee[a], Pung Swee Yong[b], Ying YuetLee[b], Nguyen Duong Ngoc Diem[a], and Lim Chin Seong[c]

[ξ]Two authors contributed equally
[a]Division of Biomedical Science, School of Pharmacy, Faculty of Science and Engineering, University of Nottingham Malaysia, Semenyih, 43500 SelangorDarul Ehsan, Malaysia;
[b]School of Materials and Mineral Resources Engineering, Engineering Campus, UniversitiSains Malaysia, 14300 NibongTebal, Penang, Malaysia;
[c]Department of Mechanical, Materials and Manufacturing Engineering, University of Nottingham Malaysia, Semenyih, 43500 Selangor Darul Ehsan, Malaysia.
*Corresponding Author: *Yuh-Fen, Pung*
Received 25 March 2020; Accepted 14 April 2020

ABSTRACT: Many studies have shown that nanoparticles such as zinc oxide (ZnO), possesses potent antimicrobial activity. This study aimed to evaluate the antifungal activity of ZnO, tungsten oxide (WO_x) nanoparticles, and the ZnO/WO_xnanohybrids against pathogenic basidiomycete fungi, *R. mucilaginosa*. Coupling of ZnO and WO_x nanoparticles was performed using liquid impregnation method. EDX analysis confirmed the presence of ZnOnanoparticles on the surface of WO_xnanoparticles. Antifungal susceptibility assays showed that ZnO nanoparticles possessed better antifungal activity as compared to WO_x and ZnO/WO_xnanohybrids (p<0.001, n=3). Time kill assay showed significant killing kinetics in ZnO NPs as compared to WO_x and ZnO/WO_xnanohybrids without UV irradiation after 5 hours (p<0.01, n=3). Interestingly, time kill assay also showed significant killing kinetics in ZnO NPs as compared WO_x and ZnO/WO_xnanohybrids as early as 1 hour after UV irradiation (p<0.001, n=3). Also, antifungal assay using semi-dry method showed no inhibitory activity, indicating the importance of release Zn^{2+} ions in the killing of fungi. Thus, our result indicated thatrelease of reactive oxygen speciesand Zn^{2+} ions were the main factors contributed to the antifungal effect. This study shed light on the potential use of ZnO NPs to coat clinical plastic ware, such as catheter, to combat catheter-related bloodstream infections associated with basidiomycete fungi.
Keywords: Zinc oxide; Tungsten oxide; Antimicrobial susceptibility tests; Minimum inhibitory concentration; Time-kill kinetic assays

Abbreviations: ZnO, Zinc Oxide; WO_x, Tungsten Oxide; NPs, nanoparticles; NHs, nanohybrids; MIC, Minimum inhibitory concentration; MFC, Minimum fungicidal concentration; ROS, reactive oxygen species; DI, deionized water; FESEM, Field emission scanning electron microscopy; FTIR, Fourier-transform infrared spectroscopy; XRD, X-ray diffraction analysis; EDX, Energy dispersive X-ray spectroscopy; % T, Percentage of transmittance; ultraviolet, UV.

I. INTRODUCTION

According to the World Health Organization in 2011, the overall prevalence of healthcare-associated infections (HAIs) in Malaysia was 14 %, which was one of the top 5 among the developing countries from 1995 to 2010[1]. Furthermore, out of RM4.3billion spent for healthcare sector in Malaysia, approximately RM640.7million (14.9% of the healthcare budget) was used for curative treatments including the use of antibiotics, chemotherapy and surgeryfor patients [2].

The increased use of implantable medical devices, such as intravascular catheters, central venous catheters and neurosurgical catheters,has led to microbial growth and biofilm formation in the lumen of catheter, thereby increasing the risk of patients to bloodstream infections which isalso known as catheter-related bloodstream infections (CRBSIs)[3–5].An additional 6 days of ICU stay was reported in a study of 100 patients diagnosed with CRBSIs which was caused by the use of contaminated catheters [6]. One specific example is CRBSIs originated from pathogenic fungi and bacteria including *Candida albicans, Rhodotorula species, Staphylococcus aureus* as well as coagulase-negative *staphylococci*[7,8].*Rhodotorula*species are categorized as basidiomycete fungi that can be found from the environment including soil, water, contaminants even food and

beverages[9]. To date, there are 8 *Rhodotorula*species that are found to be pathogenic to human. These include*R. mucilaginosa* (formerly known as *R. rubra*), *R. glunitis* and *R. minuta*[9].

Numerous cases involving *R. mucilaginosa*-associated catheter infections had been reported. Patients who suffered from meningitis, endocarditis and kidney problems,were more susceptible to infections caused by *R. mucilaginosa*[10–16]. Although antibiotics, such as amphotericin B and fluconazole, have been used as the first line therapy, resistant*R. mucilaginosa* was also evolved with the increasing use of antibiotic[17]. Thus, an alternative approach is urgently needed to prevent the infectionsassociated with resistant *R. mucilaginosa*[13,18,19].

Nanoparticles (NPs), such as ZnO, titanium oxide (TiO_2), tin dioxide (SnO_2) and silver oxide (AgO), are widely used in the semiconductor industries [20–22]. These NPs have also been reported to possess potent antimicrobial activity against fungi including*Bipolarissorokiniana*, *Magnaporthe*grisea;and bacteria including*Escherichia coli* and *Staphylococcus aureus*, respectively[20–22]. Mechanisms of the antimicrobial activity of ZnO NPs have been studied extensively in the recent decades. These mechanisms include: i) generation of reactive oxygen species (ROS) from NPs, ii) released of metal ions from NPs, and iii) interaction of NPs with cell walls[3,23]. Generation of ROS was reported to derive from the photocatalytic properties of ZnO NPs [24]. The killing mechanism involving ROS is of great interest,as it does not trigger the common pathways associated with antibiotic resistance.This gives rise to the possibility that NPs could be an alternative coating materials insidethe catheter to prevent infection related to CRBSIs[25].

Recently, doping of ZnO NPs with other transition metals such as copper[26], nickel[27], silver[28], gold[29] and cobalt[30]has become as an emerging trend. These nanohybridsexhibit enhanced antimicrobial properties. Thus, thisstudy aimed to investigate the antifungal activity of custom synthesisedZnO NPs, WO_x NPs and their hybrids against*R. mucilaginosa*. It is hope that ZnO NPs and its hybrids with WO_x NPs could represent an alternative or even complementary to antibiotics to combat CRBSIs in the near future.

II. MATERIALS AND METHODS

Synthesis of ZnO NPs

The synthesis of ZnO NPs was carried out viathe solution precipitationmethod with modifications[31]. The ZnO NPs were synthesised using 0.12 Mzinc nitrate tetrahydrate ($Zn(NO_3)_2$•$4H_2O$) (Merck, Germany), 0.12 M hexamethylenetetramine ($C_6H_{12}N_4$) (EMSURE®,Germany) and 0.4 g polyvinylpyrrolidone (PVP) (Sigma-Aldrich, Germany). The dissolving and stirring process of zinc nitrate tetrahydrate, hexamine and PVP were carried out separately in 200ml of de-ionized (DI) waterunder room temperature for 2 h. The zinc nitrate tetrahydrate and hexamine solutions were then added simultaneously to PVP solution withcontinuous mixing under the same conditions for another 1 h to completely dissolve the solutions. The solution was placed in water bath at 90°C for 45 min prior to leaving it overnight at room temperature. The washing process withDIwater and ethanol (John Kollin Corporation, UK) was carried out the next day. The whiteZnO NPs powder was collected after drying in the oven at 100 °C after 24 h.

Synthesis of WO_x NPs

The WO_x NPs weresynthesisedusing sodium tungstate dihydrate (Na_2WO_4•$2H_2O$) (Bio Basic Inc., Canada)and hydrochloric acid (HCl) (Fisher Scientific, UK) via solution precipitation method[32]. 0.4M of sodium tungstate dehydrate was dissolved in 200ml of DIwaterand stirred at 90 °C for 2 h prior to the addition of 3M hydrochloric acid in dropwise and stirring for another 2 h. The solution was then kept in water bath at 90 °C for 21 h. The precipitation settled down at room temperature overnight. The washing process for WO_x NPs was conducted with DIwater and ethanol. The yellowishWO_x NPs powder were collected after continuous drying in the oven at 100°C for 24 h.

Synthesis of ZnO/WO_x NHs

The ZnO/WO_xNHs consisted ofZnO and WO_x NPs were synthesised by liquid impregnation method by adding WO_x powder into zinc nitrate tetrahydrate to undergo hybridization of ZnO with WO_x based on the protocolwith modifications[33]. Three sets of ZnO/WO_xNHs were synthesised by having different stirring times of 24, 48 and 72 h, respectively, to obtain varied ZnO/WO_xNHs compositions. To do this, 0.12M zinc nitrate tetrahydrate was first dissolved and stirred in DIwater at room temperature for 2 h. Subsequently, 0.3g of synthesised yellow WO_x NPs powder was added in dropwise manner and continued stirring at room temperature for 24 h (Type 1ZnO/WO_xNHs), 48 h (Type 2ZnO/WO_xNHs) and 72 h (Type 3ZnO/WO_xNHs) accordingly to obtain different structural geometries. The solutions were then kept overnight to form precipitates. Several cycles of washing process using DI water andethanol were conducted for each types of ZnO/WO_xNHs. The yellow ZnO/WO_xNHs powder were collected after drying in the oven at 45°C for 24 h.

Physical and chemical characterizations of NPs and ZnO/WO_xNHs

The atomic and molecular structure of the NPs and ZnO/WO_x NHs were characterized using X-ray powder diffraction (XRD) Bruker D8 Advance diffractometer (Bruker, Germany) with Cu K_α, λ = 0.154 nm radiation in the 2 theta (2θ) scanning range from 20 °C to 80 °C. The morphologies of these nanomaterials were analysed using field emission scanning electron microscope (FESEM) Zeiss Supra 35 VP instrument (Zeiss, Germany). The bond stretching vibrations of the functional groups were recorded with fourier-transform infrared spectroscopy (FTIR) spectrum, using Mid-IR with Attenuated Total Reflectance spectrometer (ATR) (PerkinElmer, USA) in the wavenumber rangingfrom 400 to 4000cm^{-1} at 8 scans per spectrum at a resolution of 2cm^{-1}. On the other hand, the chemical element composition of ZnO NPs, WO_xNPs and ZnO/WO_xNHs were analysed through energy dispersive X-ray spectroscopy (EDX) Zeiss Supra 35 VP (Zeiss, Germany).

Assessment of antifungal activity ofZnO NPs, WO_x NPs and their NHs against Basidiomycete fungus using two-fold broth micro-dilution method

The antifungal activity of theZnO NPs, WO_x NPs and theirNHs against *R.mucilaginosa*(ATCC66034) was conducted using two-fold broth microdilution method to determine the minimum inhibitory concentration (MIC) and minimum fungicidal concentration (MFC) [34]. The MIC was defined as the lowest concentration ofZnO NPs, WO_xNPs and ZnO/WO_xNHs that inhibit the growth of *R. mucilaginosa*. The MFC was defined as the lowest concentration of ZnO NPs, WO_xNPs and ZnO/WO_xNHs that completely kill the fungal colonies withno visible growth of *R. mucilaginosa* on Sabouraud Dextrose Agar (SDA). The fungal strain, *R. mucilaginosa*was characterised using gram stain prior to the antifungal susceptibility test (**Supplementary Supplementary Figure**). Both MIC and MFC assays were performed without UV irradiation(without UV) and with UV irradiation for 60 min (60min UV). The purpose of UV irradiation exposure was to promote the release of ROSfrom the ZnO NPs, WO_xNPs andZnO/WO_x NHs. Three replicates were performed for each MIC and MFC assays to ensure consistency of the results.

Firstly,all NPs and NHs suspensions were prepared according to Soh et al. 2018 with modifications[22]. ZnO NPs, WO_xNPs and ZnO/WO_xNHs were added with sterile DI to make up a concentration of 8.192mg/ml. Subsequently, the suspensions were sonicated using ultrasound (100W, 40kHz) at 30 °C for 30 min before adding to the sterile 96-well U-bottom microplate. This sonication was performed to break down the agglomerates of NPs.

Fungal colonies of *R. mucilaginosa* were cultured in Sabouraud Dextrose broth (SDB) (Pronadisa, Spain) at 37°C overnight. The absorbance of 1 ml of fungal culture was adjusted to 0.1 at wavelength 530 nm (OD_{530}) which corresponded to approximately 1 x 10^6 colonies forming unit per millilitre (cfu/ml). 10-fold serial dilution was then performed for the fungal suspension to acquire cell density of 1x10^5cfu/ml. 100µl of the fungal suspension was added to each well of the microplates that contain equal volume of serially diluted ZnONPs, WO_x NPs andZnO/WO_x NHs. The final inoculum of fungal in each well were 5x10^4cfu/ml, and the concentration used forZnO NPs, WO_xNPs and ZnO/WO_xNHs rangedfrom16 µg/ml to 2048µg/ml. 32µg/ml of amphotericin B was added with fungal suspension to serve as the positive control while fungal suspension with solely SDB served as negative control.

For treatment that required UV irradiation, the microplates were exposed to the UV lamp for 60 min prior to the inoculation of100µl fungal suspension. Then all microplates with and without UV irradiation were incubated at 37 °C for 24 h. The MIC value of each NPs andZnO/WO_x NHs was determined.The MFC assay was performed subsequently on the SDA. The SDA was incubated at 37 °C for 24 h.

Assessment of inhibitory kineticsof ZnO NPs, WO_xNPs and ZnO/WO_x NHs against Basidiomycete fungus using time kill assay

Following the MIC and MFC assays, the inhibitory activitykinetics of all NP and NHs on *R. mucilaginosa* were studied using time kill assay with modifications[34]. The concentration of all NPs and NHs used were set at 32 µg/ml. Similar to the MIC assay, the microplates with NPs and NHs suspension were exposed to60 min UV irradiation and without UV irradiation. The time kill assay was performed for 5 h. At each 1 h interval (t = 0, 1, 2, 3, 4 and 5 h), 10µl of the sample was serially diluted in SDB before spreading onto SDA for viable colony counts. Only colonies between 20 and 200 per plate would be considered as valid range for total colony calculation. Time kill assay was repeated at least three times.

The fungal growth curve was plotted with logarithmic cfu/ml against time to investigate the inhibitory effect of NPs and NHs[35]. All data were analysed and expressed as mean ± standard error of mean (SEM). Statistical analysis was performed using One Way ANOVA followed by the Tukey's multi-comparison test from GraphPad Prism version 7.02 software (GraphPad Inc., USA). * denotes statistically significance when p<0.05.

III. RESULTS AND DISCUSSIONS

Physical and chemical characterizations of ZnO NPs, WO_x NPs and ZnO/WO_x NHs

XRD was used to detect the molecular structures ofZnO NPs, WO_x NPs and ZnO/WO_x NHs[36]. The diffraction peaks could be indexed to hexagonal phase wurzite structure of ZnO NPs (ICDD Reference Code: 98-002-8869) as shown in **Figure 1a**. The diffraction peaks observed at 31.7°, 34.4°, 36.2°, 47.5°, 56.5°, 62.8°, 66.3°, 67.9°, 69.0°, 72.5°, and 76.9° were correspond to (100), (002), (101), (102), (110), (103), (200), (112), (210), (004) and (202) crystal planes of hexagonal ZnO, respectively. No diffraction peaks of impurities were observed[37]. The peaks with the highest intensities at (100), (002) and (101) of ZnO NPs demonstrated that the ZnO NPs synthesised were of the highestquality [31]. The formation of wurtzite structure could be due to the arrangement of oxygen atoms in a packed hexagonal with zinc atoms, occupying half the tetrahedral sites.

As for WO_x NPs, there were two sets of diffraction peaks that could be indexed to WO_3 (ICDD Reference Code: 98-000-6556) and W_5O_{14} (ICDD Reference Code: 98-000-0815). Therefore, WO_x NPs was a mixture of WO_3 (lattice constant of a = 7.306 Å, b = 7.54 Å, c = 10.5269 Å, α = γ = 90 °, β = 133.062°) and tetragonal W_5O_{14} (lattice constant of a = b= 23.33 Å, c = 3.797 Å, α = β = γ = 90°). Whereas, Type 1 to Type 3 ZnO/WO_xNHs were composited with Zn^{2+} ions showed no prominent difference in 2 theta (2θ) values.

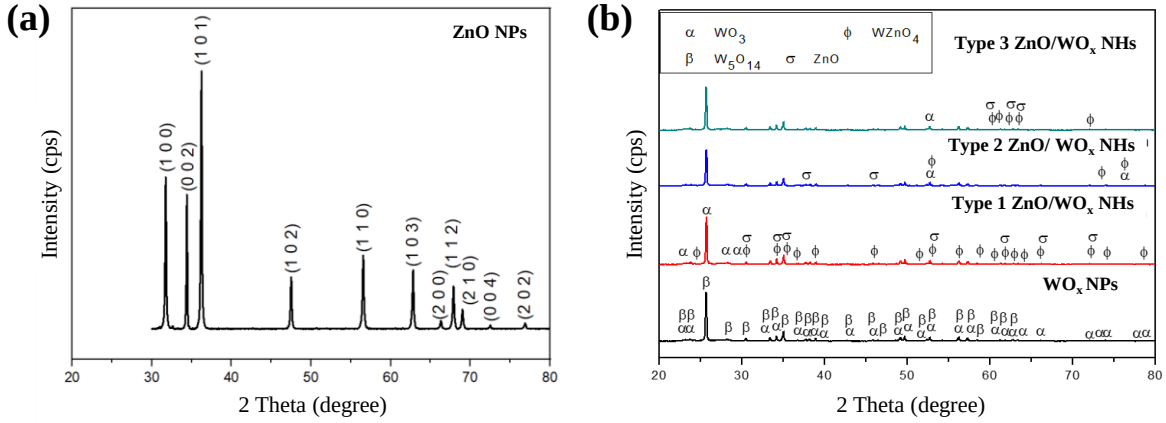

Figure 1. XRD analysis of (a)ZnO NPs, (b) WO_x NPs andthe three types of ZnO/WO_x NHs.

Based on the Rietveld refinement method, percentages of WO_3, W_5O_{14}, WZnO and ZnO that were present in the WO_x NPs and ZnO/WO_x NHs were shownin **Figure 2**. Among theZnO/WO_x NHs, Type 2 ZnO/WO_xNHs possessed the most composition of WO_3 (35%) whereas Type 3 ZnO/WO_xNHs possessed the least (27%). AllZnO/WO_x NHs generally contained more than 40% of ZnOdue to the presence of zinc nitrate tetrahydrate in the synthesis of NHs. In fact, as ZnO/WO_x NHs were prepared at longer deposition duration, the accumulation effect of ZnO NPs that deposited onto the surface of WO_x NPs was improved. The presence of $WZnO_4$ had revealed the successful deposition of ZnO onto the WO_x NPs in all Type 1 to Type 3 ZnO/WO_x NHs at 21 %, 23 % and 18%, respectively **(Figure 2b, 2c and 2d)**.According to Remškar et al. and Zheng et al., W_5O_{14} was one of the tungsten oxides phases known to have various WO_{3-x} species. W_5O_{14} possessed different oxidation states as compared to WO_3[36, 37]. This might suggest that W_5O_{14} could probably convert into WO_3 during different stirring time and resulted in the absence of W_5O_{14} in all theZnO/WO_xNHssynthesised. Based on the analysis above, it could be deduced that the intensity ratio of the crystalline phase ofZnO/WO_x NHs were similar to each other. Therefore, different stirring duration did not have prominent effect on the compositional structure of the ZnO/WO_xNHs.

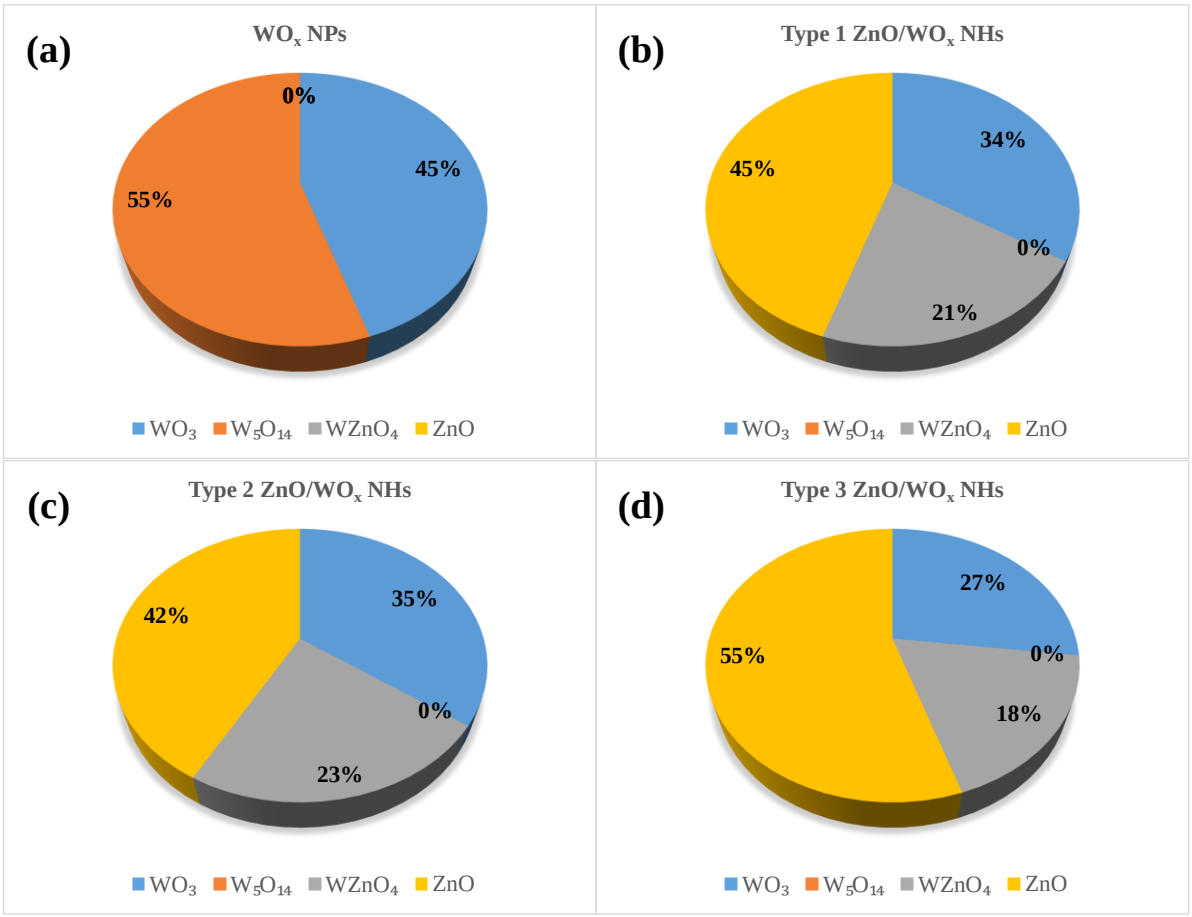

Figure 2. EDX analysis of (a)WO_x NPs and (b)-(d)ZnO/WO_x NHs.

The morphologies of ZnO NPs, WO_x NPs and allZnO/WO_x NHs were characterized by FESEM at 30 kX magnification**(Figure 3)**. ZnO NPs exhibited rod-like structure with hexagonal tip with average length and diameter of 1508.X± 273.1 nm and 208.3± 77.7 nm, respectively **(Figure 3a)**. Irregular shapes were observed in WO_x NPs with an average length of 243.48 ± 92.56 nm **(Figure 3b)**. No notable differences were observed between WO_x NPs and all 3 types ofZnO/WO_xNHs in terms of the morphologies. As shown in**Figure 3c**, **3d** and **3e**, all ZnO/WO_xNHs (Type 1, Type 2 and Type 3 ZnO/WO_xNHs) were similar to each other in terms of sizes with average length of 269.3 ± 139.0 nm, 239.76 ± 98.24 nm, 239.48 ± 83.52 nm, respectively.The stack arrangement of ZnO was probably resulted by the (002) polar surface that comprised positively-charged Zn^{2+}-terminated surface and negatively charged O^{2-}-terminated surface[39,40]. According toBojarska et al.,the hexagonal wurtzite structure of ZnO NPs was favourable for its antimicrobial properties as it significantly increases the surface to volume ratio [40]. However, FESEM images did not show prominent morphological differences between each ZnO/WO_x NHs. TheWO_x NPs showed high similarity in morphology as compared to those synthesised byMohammadi et al. [41].

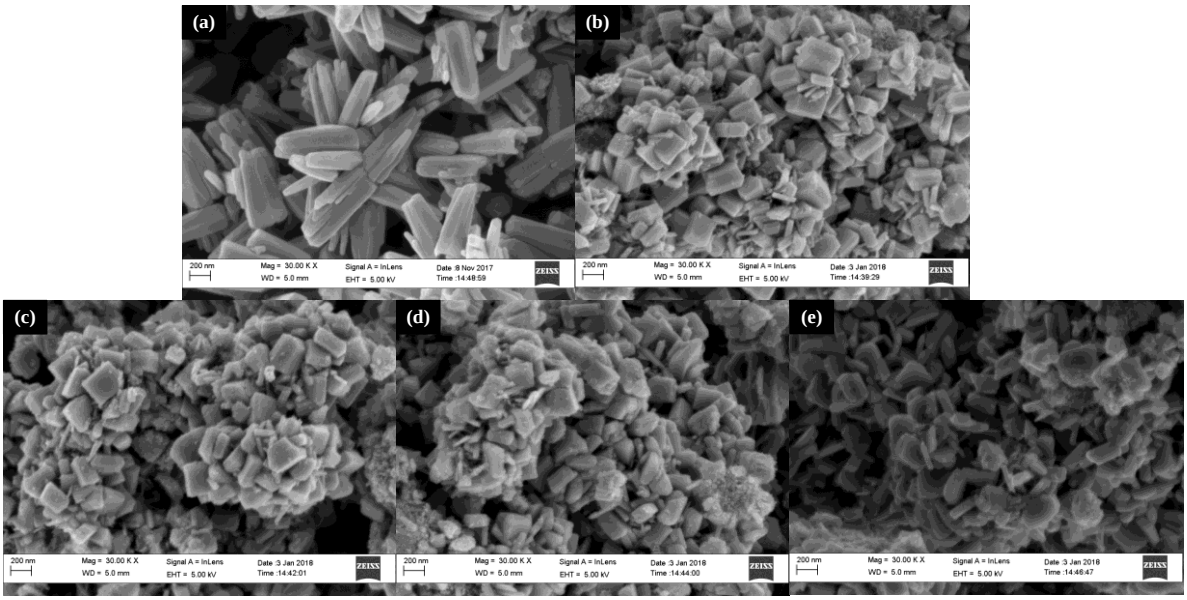

Figure 3. FESEM images of the custom-synthesised(a) ZnO NPs, (b) WO_x NPs and allZnO/WO_x NHs, (c) Type 1 ZnO/WO_x NHs, (d) Type 2 ZnO/WO_x NHs and (e) Type 3 ZnO/WO_x NHs at 30 kX magnifications. All ZnO/WO_x NHs were synthesised by liquid impregnation method with Zn^{2+} ions custom-engineered on the outer surface of WO_x NPs.

The chemical bonds of functional groups of each NPs and ZnO/WO_x NHs were performed by FTIR analysis and recordedas shown in **Figure 4**. The broad band at 524.32 cm^{-1} showed that the Zn—Obond stretching vibrations. This was comparable with several studies as the IR band of Zn—O were found within the range from 400 cm^{-1} and 670 cm^{-1}[41–46] and it was highly similar to the study from Musić, Dragčević and Popović at wavenumber 553.X cm^{-1}[47].

The stretching vibrations of O—H showed as broad band at around 3384 cm^{-1} absorption spectra. The absorption spectra of sharp peaks at around 1617 cm^{-1} were attributed to O—H bending modes of the absorbed water[32]. The stretching band at 611.82 cm^{-1} with an additional peak at 935.11 cm^{-1}observed in WO_x NPs indicated the —W—O—O— stretching vibrations [32].Intensive peak values recorded at 609.72 cm^{-1}, 608.15 cm^{-1}, 611.17 cm^{-1} and 936.81 cm^{-1}, 936.65 cm^{-1}, 936.13 cm^{-1} for Type 1 to Type 3 ZnO/WO_xNHs, respectively showed —W—O—O— stretching vibrations. The presence of broad band and two peaks observed in WO_x NPs indicated different mode of O—W—O stretching vibration in the WO_x crystal lattice[32]. The stretching vibrations of W—O single bond were detected within the range of wavenumbers 500 cm^{-1} to 900 cm^{-1} whereas the asymmetric stretching vibrations of W=O double bond was detected at approximately wavenumber 900 cm^{-1}[48–51]. FTIR bands of WO_x NPs and all ZnO/WO_x NHs synthesised in this study were collaborated to the other studies[48–51]. In brief, the spectrum observed agreed with the literature as the absorption bands of metal oxides commonly give a fingerprint region below 1000 cm^{-1}, resulting from inter-atomic vibrations [43]. The inconsistency of IR spectra of NPs was eliminated by using same amount of samples on the scanning platform of Mid-IR with ATR[52].

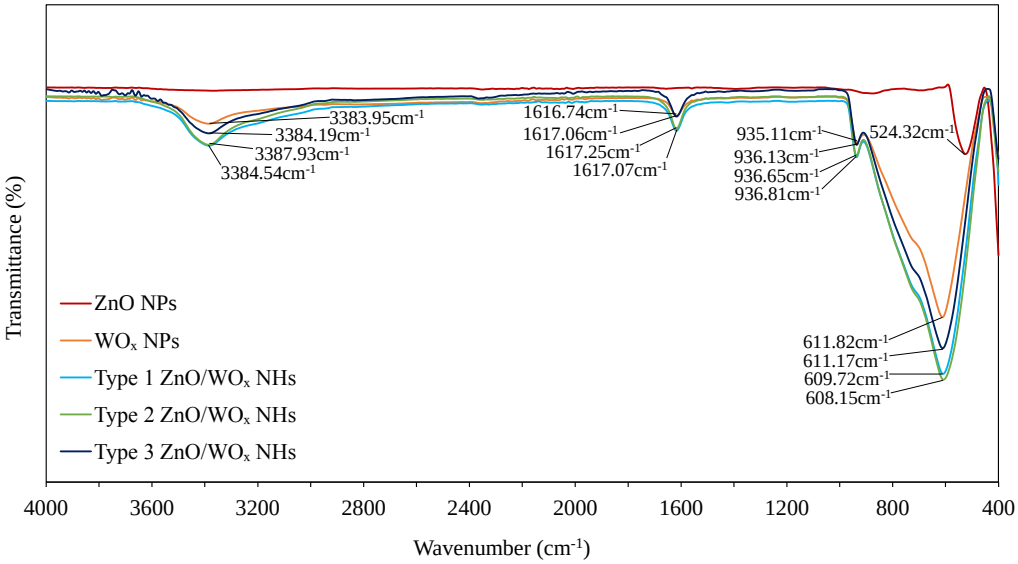

Figure 4. FTIR analysis of the custom-synthesisedZnO NPs, WO_x, NPs and ZnO/WO_xNHs.

Assessment of antifungal activity of ZnO NPs, WO_xNPs and ZnO/WO_xNHs against Basidiomycete fungus using two-fold broth microdilution method

The antifungal susceptibility tests of ZnO NPs, WO_x NPs and the three types ofZnO/WO_x NHs were performed with concentrations ranging from 16 to 2048 µg/ml without and with 60 min UV irradiation. The values of MIC and MFC of ZnO NPs, WO_x NPs and all ZnO/WO_x NHs were determined and tabulated as shown in **Table 1**. The coupling of different metal oxide semiconductors was to improve photocatalytic activity by promoting electron-hole pairs separation and reducing the recombination rate of electron-hole pairs. In this study, ZnO NPs was coupled with WO_x NPs under different stirring duration to produce three types of ZnO/WO_x NHs. This was performed to determine any enhancement in antifungal properties against *R. mucilaginosa* according to their photocatalytic performance under UV irradiation.

In **Table 1**, ZnO NPs shows the lowest MIC value (32 µg/ml) in inhibiting the growth of *R. mucilaginosa* among all the NPs without UV irradiation. The MIC value of WO_x (2048 µg/ml) was found to be 64-fold higher than that of ZnO NPs. Both Type 2 and Type 3 ZnO/WO_x NHs possessed two-fold lower MIC value (1024 µg/ml) against *R. mucilaginosa* as compared to Type 1 ZnO/WO_x NHs (2048 µg/ml). The MFC value of ZnO NPs was the lowest, 64 µg/ml and 32 µg/ml without UV irradiation and with 60min UV irradiation, respectively. ZnO NPs showed improved fungicidal effect with two-fold lower MFC value after 60min UV irradiation. The improved fungicidal effect might be due to the ROS production from ZnO NPs upon UV irradiation. WO_x NPs showed no fungicidal effect (> 2048 µg/ml) after 60min UV irradiation. There was limited study on the antifungal activity of WO_x NPs reported in the recent decades. However,one study by Ying et al.reported a similar minimum bactericidal concentration (> 2048 µg/ml) of WO_x NPs against *Bacillus subtilis* and *Staphylococcus aureus*after 2 h of UV irradiation[32].

Both Type 2 and Type 3 ZnO/WO_x NHs demonstrated better fungicidal effect (1024 µg/ml) than Type 1 ZnO/WO_x NHs (2048 µg/ml). Type 2 and Type 3 ZnO/WO_x NHs that were synthesised with longer stirring duration showed better fungicidal effect than Type 1 ZnO/WO_x NHs. However, the coupling of ZnO/WO_x NHs did not show a more potent antifungal activity than that of ZnONPs alone even though the deposition of ZnO NPs was on the surface of WO_x NPs.

In other study, He et al.reported that the MIC value of ZnOnanorods against *Botrytis cinerea* and *Penicilliumexpansum* was greater than 3 $mmolL^{-1}$ (approximately 244.24 µg/ml)[53]. Although the size ofZnO NPs synthesised in this study was greater, the MIC value was 15-fold lower than other study[53]. This could be due to the photocatalytic properties of our ZnOnanorods, which was better than ZnO NPs with other morphologies[54]. Additionally, a recent study using *Colletotrichumgloeosporioides*treated with ZnO NPs was found to have MIC value between 156 and 312 µg/ml [55]. In short, the results from MIC and MFC assays demonstrated that ZnO NPssynthesised in this study showed improvedantifungal activity in comparison to other studies[53,55–57].

Table 1. Minimum inhibitory concentration (MIC) and minimum fungicidal concentration (MFC) of ZnO NPs, WO_xNPs and ZnO/WO_xNHs against *R. mucilaginosa* (ATCC66034).

	Without UV		60 min UV	
	MIC (µg/ml)	MFC (µg/ml)	MIC (µg/ml)	MFC (µg/ml)
ZnO NPs	32	64	32	32
WO_x NPs	2048	2048	2048	(-)
Type 1 ZnO/WO_xNHs	2048	2048	2048	1024
Type 2 ZnO/WO_xNHs	1024	1024	1024	1024
Type 3 ZnO/WO_xNHs	1024	1024	1024	1024

5 x 10^4cfu/ml; n = 3; (-) denotes no fungicidal activity of NPs observed.

Assessment of inhibitory kinetics ofZnO NPs, WO_xNPs and ZnO/WO_x NHs against Basidiomycete fungus using time kill assay

Following the antifungal susceptibility assay, time kill assay was performed to determine the kinetics of inhibition of all NPs and NHs against *R. mucilaginosa*. ZnO NPs showed significant differences in inhibitory activity as compared toWO_x and all 3 types ofZnO/WO_x NHs (n = 3, p<0.001) as early as t = 1 h onwards(**Figure 5**). ZnO NPs was able to inhibit the growth of *R. mucilaginosa* completely after the first hour of treatment without UVirradiation. The results also clearly showed that the fungicidal activity of ZnO NPs after 60min UV irradiation was more potent against *R. mucilaginosa* as shown in **Figure 5b**. The inhibitory effects of WO_x NPs and all ZnO/WO_x NHs were not significant after 5 h as the fungal cell density remained consistent after treatment under both without UVirradiation and 60 min UV irradiation conditions. This result further suggested that the coupling of ZnO and WO_x NPs did not improve the antifungal activity against *R. mucilaginosa*.

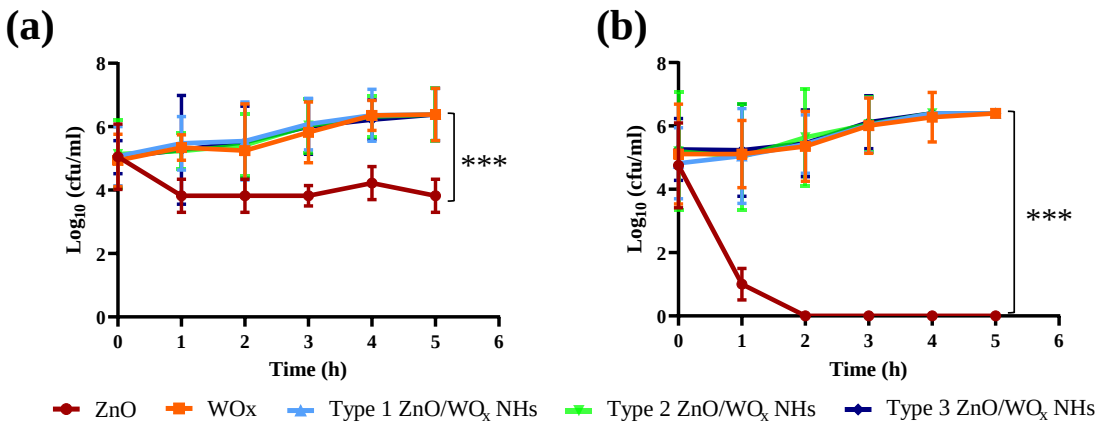

Figure 5 The kinetic study of ZnO NPs, WO_xNPs and ZnO/WO_xNHs inhibition at 32 µg/ml against *R. mucilaginosa* (ATCC 66034) without UVirradiation (a) and with 60min UV irradiation (b) over 5 h. Data were expressed as mean ± SEM (n = 3). * indicates the significant statistical differencesin antifungal activity of ZnO NPs as compared to WO_x NPs and ZnO/WO_x NHs (p<0.001; n = 3; One Way ANOVA with Tukey's multi-comparison test). This suggested the antifungal properties of ZnO NPs was due to the ROS production from ZnO NPs.**

The proposed antimicrobial mechanisms of ZnO NPsare: i) production of ROS from NPs, ii) release of metal ions such as Zn^{2+} ions, and iii) cell wall components of microorganisms involved [3,32,40]. Many studies had examined the antimicrobial activity of NPs against bacteria [23,24,58–61]whereas limited studies had used fungi as study model [62–65]. A recent study of He et al. suggested that there might be different mechanisms of inhibitory activity of ZnO NPs against fungi in comparison to those reported in bacteria[53]. This

differencescould be due to the cell wall components of fungi that are much more complicated than as seen in bacterial systems [55].

The inhibitory activity on*R. mucilaginosa* in the present study could be due to the presence of Zn^{2+} ions and ROS released from ZnO NPs. Firstly, the time kill assay and MFC assay suggested that the ROS produced from ZnO NPs exerted enhanced fungicidal effect on *R. mucilaginosa* after 60min UV irradiation. ROS, such as hydrogen peroxide (H_2O_2), hydroxyl free radicals (•OH) and superoxide anion ($•O^{2-}$), are released from NPs upon excitation[66]. ROS are well-known with their ability in causing oxidative damage to the integrity of cell membrane and cellular components such as deoxyribonucleic acids (DNAs) and enzymes[40,61]. The fungal cell wall is a single cell membrane that consists of glycoproteins, amorphous β-glucan, β-glucan, chitin and inner membrane proteins[67]. The most abundant cell wall component of major fungal cell membrane is the polysaccharide known as β-glucan[68].

Thus, the potent killing effect of ZnO NPs was proposed to be associated with ROS that were in contact with the fungal cell wall, causing the oxidative damage to the cell structure of *R. mucilaginosa*. Consequently, the fungal growth was inhibited due the DNAs and proteins damage. Besides, higher MFC values of WO_x NPs and ZnO/WO_x NHs were needed to kill *R. mucilaginosa* in comparison to that of ZnO NPs. It is postulated that possibly the morphology of ZnO/WO_x NHs might have led to the insufficient ROS production. This could explain the reason of the poor antifungal activities of WO_xNPs and all ZnO/WO_x NHs as compared to ZnO NPs. It is also important to note that the amount of ROS required to kill fungi was found to be more than that of bacteria due to different cell wall structure [69].

Similar result wasobtained in which ROS was found to induce cell wall damage to *Candida albicans*[63]. Elevated carbohydrate contents afterZnO NPs treatment was reported in other study involving fungi[62]. Deformed fungal hyphae of *Botrytis cinerea* and increased level of nucleic acids and carbohydrates from fungal hyphae after ZnO NPs treatment was reported in another similar study[53].

Another proposed mechanism is the released of Zn^{2+} ions from the ZnO NPs. The heavy metal ions including Zn^{2+} from ZnO NPs, W^{6+} from WO_x NPs and ZnO/WO_x NHs were prepared in suspension to check for the antifungal activity in this study. This was because NPs and NHs prepared in semi-dry preparation did not exhibit any antimicrobial activity in our lab (data not shown). W^{6+} ions from WO_x NPs and ZnO/WO_x NHs were reported to inhibit the growth of gram-positive bacteria including *Bacillus subtilis* and *Staphylococcus aureus*[32]. However, there were no studies using fungal model to examine the antifungal activity of WO_x NPs to date. Free mobilized Zn^{2+} ions were suggested to interact with fungal cell wall composition, interrupt the transmembrane electron transport on the fungal cell membrane, leading to destruction of proteins and DNAs, and consequently cell death [40,56]. The release of Zn^{2+} ions were accountable to the antifungal activity of ZnO NPs were reported in a study with *Saccharomyces cerevisiae*[56]. Zinc (II) sulphate ($ZnSO_4$) was used as an alternative to treat the yeast and similar concentration to that of ZnO NPs (EC_{50}) was obtained. Li et al. proposed that both the release of Zn^{2+} and induction of ROS production in mitochondria by ZnO NPs are the main toxicity of ZnO NPs[70]. Yeast such as *R. mucilaginosa* are eukaryotic cells contains mitochondria that play important role in cell signalling and apoptosis [70].

Based on the suggestions above, the antifungal activity of ZnO NPs against *R. mucilaginosa* was proposed due to the release of Zn^{2+} and induction of ROS production from ZnO NPs as shown in **Figure 6**.

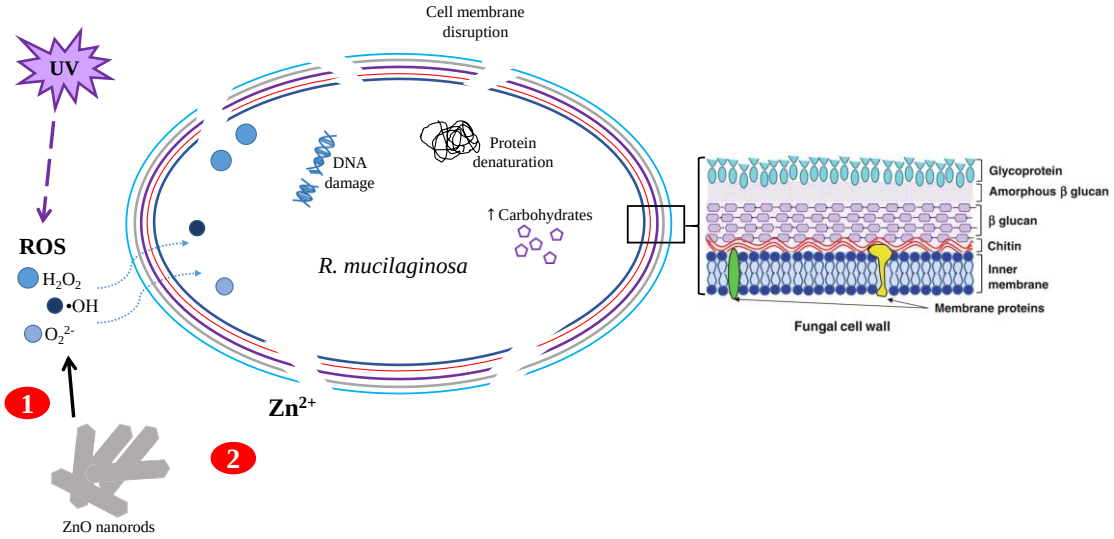

Figure 6. Proposed mechanism of antifungal activity of ZnO NPs against *R. mucilaginosa* (ATCC 66034). In the presence of UV irradiation, ROS such as hydrogen peroxide (H_2O_2), hydroxyl free radicals (•OH) and superoxide anion ($•O^{2-}$),are released from ZnO NPs upon excitation. Zn^{2+} also released from ZnO NPs as ZnO NPs were dissolved as suspension. These ROS and Zn^{2+} ionsdisrupt fungal cell wall, induce DNAs damage leading to mutated proteins production, and subsequently cell death.

IV. CONCLUSIONS

In the current study, the distinct antifungal activity of the custom-synthesisedZnO NPs in comparison to WO_x NPs and all ZnO/WO_xNHs against *R. mucilaginosa*without UV and with 60min UV irradiation was reported. ROS production from ZnO NPs upon UV irradiation contributed to the potent antifungal activity on *R. mucilaginosa*. In addition, Type 1 ZnO/WO_xNHs showed better antifungal activity in comparison to Type 2 and 3ZnO/WO_x NHs even though these NHs shared similar morphologies and properties. In addition, antifungal assay using semi-dry method showed no inhibitory activity. Thus, the findings from this study showed the importance of ROS and the release Zn^{2+} ions in the antifungal activity ZnO NPs, and also shed light on the mechanistic pathway involved. Our study suggested the potential use of ZnO NPs to coat clinical plastic ware, such as catheter, to combat CRBSIs.

ACKNOWLEDGEMENTS

This project was funded by the University of Nottingham Malaysia Research Grant (UNHD0005) and Ministry of Higher Education Grant (FRGS/1/2019/SKK08/UNIM/02/2)awarded to Yuh-Fen Pung and the UniversitiSains Malaysia Research University Grant (1001/PBAHAN/814200) awarded to Swee-Yong Pung.

REFERENCES

[1]. (WHO) World Health Organization, Report on the Burden of Endemic Health Care-Associated Infection Worldwide, 2011. https://doi.org/http://whqlibdoc.who.int/publications/2011/9789241501507_eng.pdf.

[2]. Malaysia National Health Accounts Unit Planning Division Ministry of Health Malaysia, Malaysia National Health Accounts (MNHA) Health Expenditure Report 1997-2013, Malaysia, 2015.

[3]. L. Wang, C. Hu, L. Shao, The antimicrobial activity of nanoparticles: present situation and prospects for the future, Int. J. Nanomedicine. 12 (2017) 1227–1249. https://doi.org/10.2147/IJN.S121956.

[4]. I. Raad, H. Hanna, Y. Jiang, T. Dvorak, R. Reitzel, G. Chaiban, R. Sherertz, R. Hachem, Comparative activities of daptomycin, linezolid, and tigecycline against catheter-related methicillin-resistant Staphylococcus bacteremic isolates embedded in biofilm, Antimicrob. Agents Chemother. 51 (2007) 1656–1660. https://doi.org/10.1128/AAC.00350-06.

[5]. S. Hogan, M. Zapotoczna, N.T. Stevens, H. Humphreys, J.P. O'Gara, E. O'Neill, In vitro approach for identification of the most effective agents for antimicrobial lock therapy in the treatment of intravascular catheter-related infections caused by Staphylococcus aureus, Antimicrob. Agents Chemother. 60 (2016) 2923–2931. https://doi.org/10.1128/AAC.02885-15.

[6]. a Sulong, N. Jalil, R. Ramli, M. Yusoff, Surveillance of central-line associated bloodstream infections in ICU at a Malaysian medical centre, BMC Proc. 5 (2011) P212. https://doi.org/10.1186/1753-6561-5-S6-P212.

[7]. A.H.A. Gafor, P.C. Ping, A.F.Z. Abidin, M.Z. Saruddin, N.K. Yan, S.Q.A. Adam, R. Ramli, A. Sulong,

P. Periyasamy, Antibiogram for haemodialysis catheter-related bloodstream infections, 2014 (2014) 629459. https://doi.org/10.1155/2014/629459.

[8]. A. Jaberi, A. Hadziomerovic, S.S. Toor, R.P. Galwa, J. Graham, R.E. Thornhill, S.E. Ryan, Externalization of tunneled hemodialysis catheter in patients with tunnel or exit-site infections and limited access options, J. Vasc. Interv. Radiol. 25 (2014) 561–566. https://doi.org/10.1016/j.jvir.2013.12.570.

[9]. F. Wirth, L.Z. Goldani, Epidemiology of rhodotorula: An emerging pathogen, Interdiscip. Perspect. Infect. Dis. 2012 (2012) 465717. https://doi.org/10.1155/2012/465717.

[10]. O.H. Gyaurgieva, T.S. Bogomolova, G.I. Gorshkova, Meningitis caused by Rhodotorula rubra in an HIV-infected patient, 1996.

[11]. J.W. Chung, B.N. Kim, Y.S. Kim, Central venous catheter-related Rhodotorula rubra fungemia, J. Infect. Chemother. 8 (2002) 109–110. https://doi.org/10.1007/s101560200017.

[12]. K. Thakur, G. Singh, S. Agarwal, L. Rani, Meningitis caused by Rhodotorula rubra in an human immunodeficiency virus infected patient, Indian J. Med. Microbiol. 25 (2007) 166–168.

[13]. G.M.D.D.E. Almeida, S.F. Costa, M. Melhem, A.L. Motta, M.N. Burattini, Rhodotorula spp . isolated from blood cultures : clinical and microbiological aspects, Med. Mycol. 46 (2008) 547–556. https://doi.org/10.1080/13693780801972490.

[14]. S. Bhama, B. Paul, R. Bai, J. Theodore, S. Sugathan, Rhodotorula species from CAPD fluid, J. Acad. Clin. Microbiol. 16 (2014) 38–39.

[15]. M. Capoor, S. Aggarwal, C. Raghvan, D. Gupta, A. Jain, R. Chaudhary, Clinical and microbiological characteristics of Rhodotorula mucilaginosa infections in a tertiary-Care facility, Indian J. Med. Microbiol. 32 (2014) 304. https://doi.org/10.4103/0255-0857.136576.

[16]. T. Won Bae, J. Lee, Y. Cho, D. Sik Kim, S. Im Choi, H. Soo Lee, Sepsis Due to Rhodotorula mucilaginosa in a Patient with Advanced Non-Small Cell Lung Cancer, Lab. Med. Online. 6 (2016) 102. https://doi.org/10.3343/lmo.2016.6.2.102.

[17]. A.K. Zaas, M. Boyce, W. Schell, B.A. Lodge, J.L. Miller, J.R. Perfect, Risk of Fungemia Due to Rhodotorula and Antifungal Susceptibility Testing of Rhodotorula Isolates, J. Clin. Microbiol. 41 (2003) 5233–5235. https://doi.org/10.1128/JCM.41.11.5233-5235.2003.

[18]. D.M. Sievert, P. Ricks, J.R. Edwards, A. Schneider, J. Patel, A. Srinivasan, A. Kallen, B. Limbago, S. Fridkin, Antimicrobial-Resistant Pathogens Associated with Healthcare-Associated Infections Summary of Data Reported to the National Healthcare Safety Network at the Centers for Disease Control and Prevention, 2009–2010, Infect. Control Hosp. Epidemiol. 34 (2013) 1–14. https://doi.org/10.1086/668770.

[19]. M.S. Simon, S. Somersan, H.K. Singh, B. Hartman, B.L. Wickes, S.G. Jenkins, T.J. Walsh, A.N. Schuetz, Endocarditis caused by rhodotorula infection, J. Clin. Microbiol. 52 (2014) 374–378. https://doi.org/10.1128/JCM.01950-13.

[20]. Y.-K. Nasrollahi, B.H. Kim, G. Jung, Antifungal Activity of Silver Nanoparticles on some fungi, Plant Dis. 93 (2009) 1037–1043. https://doi.org/10.1094/PDIS-93-10-1037.

[21]. S.M. Amininezhad, A. Rezvani, M. Amouheidari, S.M. Amininejad, S. Rakhshani, The Antibacterial Activity of SnO2 Nanoparticles against Escherichia coli and Staphylococcus aureus, Zahedan J. Res. Med. Sci. 17 (2015) e1053. https://doi.org/10.17795/zjrms-1053.

[22]. S. Fanny Chiat Orou, J.H. Kee, M.T. Thien, Y.L. Ying, C.F. Le, D.N.D. Nguyen, B.H. Goh, S.Y. Pung, Y.F. Pung, Antibacterial activity by ZnO nanorods and ZnO nanodisks: A model used to illustrate "Nanotoxicity Threshold," J. Ind. Eng. Chem. 62 (2018) 333–340. https://doi.org/10.1016/j.jiec.2018.01.013.

[23]. Y. Li, W. Zhang, J. Niu, Y. Chen, Mechanism of photogenerated reactive oxygen species and correlation with the antibacterial properties of engineered metal-oxide nanoparticles, ACS Nano. 6 (2012) 5164–5173. https://doi.org/10.1021/nn300934k.

[24]. N. Padmavathy, R. Vijayaraghavan, Enhanced bioactivity of ZnO nanoparticles - An antimicrobial study, Sci. Technol. Adv. Mater. 9 (2008). https://doi.org/10.1088/1468-6996/9/3/035004.

[25]. H. Teterycz, P. Suchorska-Woźniak, M. Fiedot, I. Karbownik, Deposition of Zinc Oxide on the Materials Used in Medicine. Preliminary Results, FIBRES Text. East. Eur. 22 (2014) 3–126.

[26]. I.A. Hassan, S. Sathasivam, S.P. Nair, C.J. Carmalt, Antimicrobial Properties of Copper-Doped ZnO Coatings under Darkness and White Light Illumination, ACS Omega. 2 (2017) 4556–4562. https://doi.org/10.1021/acsomega.7b00759.

[27]. S.B. Rana, R.P.P. Singh, Investigation of structural, optical, magnetic properties and antibacterial activity of Ni-doped zinc oxide nanoparticles, J. Mater. Sci. Mater. Electron. 27 (2016) 9346–9355. https://doi.org/10.1007/s10854-016-4975-6.

[28]. N. Sharma, J. Kumar, S. Thakur, S. Sharma, V. Shrivastava, Antibacterial study of silver doped zinc

oxide nanoparticles against Staphylococcus aureus and Bacillus subtilis, Drug Invent. Today. 5 (2013) 50–54. https://doi.org/10.1016/j.dit.2013.03.007.
[29]. A.B.P. Jiménez, C.A.H. Aguilar, J.M.V. Ramos, P. Thangarasu, Synergistic antibacterial activity of nanohybrid materials ZnO-Ag and ZnO-Au: Synthesis, characterization, and comparative analysis of undoped and doped ZnO nanoparticles, Aust. J. Chem. 68 (2015) 288–297. https://doi.org/10.1071/CH14123.
[30]. M. Oves, M. Arshad, M.S. Khan, A.S. Ahmed, A. Azam, I.M.I. Ismail, Anti-microbial activity of cobalt doped zinc oxide nanoparticles: Targeting water borne bacteria, J. Saudi Chem. Soc. 19 (2015) 581–588. https://doi.org/10.1016/j.jscs.2015.05.003.
[31]. M.T. Thein, S.-Y. Pung, L.S. Chuah, Y.-F. Pung, Photodegradation behavior of ZnO nanorods on various types of organic dyes, Adv. Mater. Process. Technol. 4 (2018) 272–280. https://doi.org/10.1080/2374068X.2017.1416882.
[32]. Y.L. Ying, S.Y. Pung, M.T. Ong, Y.F. Pung, Rhodomine B dye removal and inhibitory effect on B. subtilis and S. aureus by WOxnanoparticles, J. Ind. Eng. Chem. 67 (2018)437-447. https://doi.org/10.1016/j.jiec.2018.07.018.
[33]. M.S.W. Yuen, A.H. Abdullah, H.N. Lim, Synthesis of ZnO/rGO Nanohybrid for Improved Photocatalytic Activity, Malaysian J. Anal. Sci. 21 (2017) 889–900. https://doi.org/10.17576/mjas-2017-2104-15.
[34]. The National Commitee for Clinical Laboratory Standards (CLSI), Reference Method for Broth Dilution Antifungal Susceptibility Testing of Yeasts; Approved Standard — Second Edition, NCCLS Doc. M27-A2. 22 (2002) 1–30.
[35]. B.E. Ferro, J. Van Ingen, M. Wattenberg, D. Van Soolingen, J.W. Mouton, Time-kill kinetics of antibiotics active against rapidly growing mycobacteria, J. Antimicrob. Chemother. 70 (2015) 811–817. https://doi.org/10.1093/jac/dku431.
[36]. A.H. Kurda, Y.M. Hassan, N.M. Ahmed, Controlling Diameter, Length and Characterization of ZnO Nanorods by Simple Hydrothermal Method for Solar Cells, World J. Nano Sci. Eng. 5 (2015) 34–40. https://doi.org/10.4236/wjnse.2015.51005.
[37]. P. Bindu, S. Thomas, Estimation of lattice strain in ZnO nanoparticles: X-ray peak profile analysis, J. Theor. Appl. Phys. 8 (2014) 123–134. https://doi.org/10.1007/s40094-014-0141-9.
[38]. J.Y. Zheng, Z. Haider, T.K. Van, A.U. Pawar, M.J. Kang, C.W. Kim, Y.S. Kang, Tuning of the crystal engineering and photoelectrochemical properties of crystalline tungsten oxide for optoelectronic device applications, CrystEngComm. 17 (2015) 6070–6093. https://doi.org/10.1039/C5CE00900F.
[39]. M.T. Thein, J.E. Chim, S.-Y. Pung, Y.-F. Pung, Highly UV light driven WOx@ZnO nanocomposites synthesized by liquid impregnation method, J. Ind. Eng. Chem. 46 (2017) 119–129. https://doi.org/10.1016/j.jiec.2016.10.022.
[40]. M. Bojarska, B. Nowak, J. Skowroński, W. Piątkiewicz, L. Gradoń, Growth of ZnO nanowires on polypropylene membrane surface—Characterization and reactivity, Appl. Surf. Sci. 391 (2017) 457–467. https://doi.org/10.1016/j.apsusc.2016.04.130.
[41]. S. Mohammadi, M. Sohrabi, A.N. Golikand, A. Fakhri, Preparation and characterization of zinc and copper co-doped WO3nanoparticles: Application in photocatalysis and photobiology, J. Photochem. Photobiol. B Biol. 161 (2016) 217–221. https://doi.org/10.1016/j.jphotobiol.2016.05.020.
[42]. Z.R. Khan, M.S. Khan, M. Zulfequar, M.S. Khan, Optical and Structural Properties of ZnO Thin Films Fabricated by Sol-Gel Method, Mater. Sci. Appl. 2 (2011) 340–345. https://doi.org/10.4236/msa.2011.25044.
[43]. H. Kumar, R. Rani, Structural and Optical Characterization of ZnO Nanoparticles Synthesized by Microemulsion Route, Int. Lett. Chem. Phys. Astron. 19 (2013) 26–36. https://doi.org/10.18052/www.scipress.com/ILCPA.19.26.
[44]. S.S. Kulkarni, S. Sawarkar Mahavidyalaya, M.D. Shirsat, Optical and Structural Properties of Zinc Oxide Nanoparticles, Int. J. Adv. Res. Phys. Sci. 2 (2015) 14–18. www.arcjournals.org.
[45]. K. Saoud, R. Alsoubaihi, N. Bensalah, T. Bora, M. Bertino, J. Dutta, Synthesis of Supported Silver Nano-spheres on Zinc Oxide Nanorods for Visible Light Photocatalytic Applications, Mater. Res. Bull. 63 (2015) 134–140. https://doi.org/10.1016/j.materresbull.2014.12.001.
[46]. K. Sowri Babu, A. Ramachandra Reddy, C. Sujatha, K. Venugopal Reddy, A.N. Mallika, Synthesis and optical characterization of porous ZnO, J. Adv. Ceram. 2 (2013) 260-265. https://doi.org/10.1007/s40145-013-0069-6.
[47]. S. Musić, Đ. Dragčević, S. Popović, Influence of synthesis route on the formation of ZnO particles and their morphologies, J. Alloys Compd. 429 (2007) 242–249. https://doi.org/10.1016/j.jallcom.2006.03.084.
[48]. H.I.S. Nogueira, A.M. V Cavaleiro, T. Trindade, Synthesis and characterization of tungsten trioxide

powders prepared from tungstic acids, Mater. Res. Bull. 39 (2004) 683–693. https://doi.org/10.1016/j.materresbull.2003.11.004.
[49]. J. Díaz-Reyes, V. Dorantes-García, Obtaining of films of tungsten trioxide (WO3) by resistive heating of a tungsten filament, Superf. y Vacio. 21 (2008) 12–17. http://www.scielo.org.mx/pdf/sv/v21n2/v21n2a3.
[50]. V. Chaudhary, A. Kaur, Enhanced room temperature sulfur dioxide sensing behaviour of in situ polymerized polyaniline–tungsten oxide nanocomposite possessing honeycomb morphology, RSC Adv. 5 (2015) 73535–73544. https://doi.org/10.1039/C5RA08275G.
[51]. S. Thangavel, M. Elayaperumal, G. Venugopal, Synthesis and Properties of Tungsten Oxide and Reduced Graphene Oxide Nanocomposites, Mater. Express. 2 (2012) 327–334. https://doi.org/10.1166/mex.2012.1087.
[52]. K. Lawson-wood, I. Robertson, S. Green, Comparison of Near- and Mid-Infrared Spectroscopy for Herb and Spice Authenticity Analysis, in: Appl. Note Near- Mid-Infrared Spectrosc., PerkinElmer Inc, USA, 2016.
[53]. L. He, Y. Liu, A. Mustapha, M. Lin, Antifungal activity of zinc oxide nanoparticles against Botrytis cinerea and Penicillium expansum, Microbiol. Res. 166 (2011) 207–215. https://doi.org/10.1016/j.micres.2010.03.003.
[54]. S.-Y. Pung, W.-P. Lee, A. Aziz, Kinetic Study of Organic Dye Degradation Using ZnO Particles with Different Morphologies as a Photocatalyst, Int. J. Inorg. Chem. 2012 (2012) 1–9. https://doi.org/10.1155/2012/608183.
[55]. S.C. De La Rosa-García, P. Martínez-Torres, S. Gómez-Cornelio, M.A. Corral-Aguado, P. Quintana, N.M. Gómez-Ortíz, Antifungal activity of ZnO and MgO nanomaterials and their mixtures against colletotrichum gloeosporioides strains from tropical fruit, J. Nanomater. 2018 (2018) 1-9. https://doi.org/10.1155/2018/3498527.
[56]. K. Kasemets, A. Ivask, H.C. Dubourguier, A. Kahru, Toxicity of nanoparticles of ZnO, CuO and TiO2 to yeast Saccharomyces cerevisiae, Toxicol. Vitr. 23 (2009) 1116–1122. https://doi.org/10.1016/j.tiv.2009.05.015.
[57]. G.D. Savi, A.J. Bortoluzzi, V.M. Scussel, Antifungal properties of Zinc-compounds against toxigenic fungi and mycotoxin, Int. J. Food Sci. Technol. 48 (2013) 1834–1840. https://doi.org/10.1111/ijfs.12158.
[58]. O. Yamamoto, Influence of particle size on the antibacterial activity of zinc oxide, Int. J. Inorg. Mater. 3 (2001) 643–646. https://doi.org/http://dx.doi.org/10.1016/S1466-6049(01)00197-0.
[59]. Y. Jiang, A.J. O'Neill, Y. Ding, Zinc oxide nanoparticle-coated films: fabrication, characterization, and antibacterial properties, J. Nanoparticle Res. 17 (2015) 180-190. https://doi.org/10.1007/s11051-015-2993-6.
[60]. C. Rode, M. Zieger, R. Wyrwa, S. Thein, C. Wiegand, M. Weiser, A. Ludwig, D. Wehner, U. Hipler, Antibacterial Zinc Oxide Nanoparticle Coating of Polyester Fabrics, J. Text. Sci. Technol. 1 (2015) 65–74. https://doi.org/10.4236/jtst.2015.12007.
[61]. S. Fanny Chiat Orou, J.H. Kee, M.T. Thien, Y.L. Ying, C.F. Le, D.N.D. Nguyen, B.H. Goh, S.Y. Pung, Y.F. Pung, Antibacterial activity by ZnO nanorods and ZnO nanodisks: A model used to illustrate "Nanotoxicity Threshold," J. Ind. Eng. Chem. 62 (2018) 333–340. https://doi.org/10.1016/j.jiec.2018.01.013.
[62]. K.J. Kim, W.S. Sung, B.K. Suh, S.K. Moon, J.S. Choi, J.G. Kim, D.G. Lee, Antifungal activity and mode of action of silver nano-particles on Candida albicans, BioMetals. 22 (2009) 235–242. https://doi.org/10.1007/s10534-008-9159-2.
[63]. A. Lipovsky, Y. Nitzan, A. Gedanken, R. Lubart, Antifungal activity of ZnO nanoparticles-the role of ROS mediated cell injury, Nanotechnology. 22 (2011). https://doi.org/10.1088/0957-4484/22/10/105101.
[64]. E.M. El-Diasty, M.A. Ahmed, N. Okasha, S.F. Mansour, S.I. El-Dek, H.M.A. El-Khalek, M.H. Youssif, Antifungal activity of zinc oxide nanoparticles against dermatophytic lesions of cattle, Rom. J. Biophys. 23 (2013) 191–202.
[65]. E.M. Maiolo, A. Oliva, U. Furustrand Tafin, N. Perrotet, O. Borens, A. Trampuz, Antifungal activity against planktonic and biofilm Candida albicans in an experimental model of foreign-body infection, J. Infect. 72 (2016) 386–392. https://doi.org/10.1016/j.jinf.2015.12.008.
[66]. K. Akhil, J. Jayakumar, G. Gayathri, S.S. Khan, Effect of various capping agents on photocatalytic, antibacterial and antibiofilm activities of ZnO nanoparticles, J. Photochem. Photobiol. B Biol. 160 (2016) 32–42. https://doi.org/10.1016/j.jphotobiol.2016.03.015.
[67]. L. Brown, J.M. Wolf, R. Prados-Rosales, A. Casadevall, Through the wall: extracellular vesicles in Gram-positive bacteria, mycobacteria and fungi, Nat. Rev. Microbiol. 13 (2015) 620-630. https://doi.org/10.1038/nrmicro3480.
[68]. P.H. Fesel, A. Zuccaro, β-glucan: Crucial component of the fungal cell wall and elusive MAMP in plants, Fungal Genet. Biol. 90 (2016) 53–60. https://doi.org/https://doi.org/10.1016/j.fgb.2015.12.004.

[69]. T.N. Demidova, M.R. Hamblin, Effect of cell-photosensitizer binding and cell density on microbial photoinactivation, Antimicrob. Agents Chemother. 49 (2005) 2329–2335. https://doi.org/10.1128/AAC.49.6.2329-2335.2005.
[70]. J. Li, Q. Yu, G. Zhao, Y. Zhang, Y. Liu, F. Jiang, X. Liu, F. Tian, Toxicity of nano zinc oxide to mitochondria, Toxicol. Res. (Camb). 1 (2012) 137–144. https://doi.org/10.1039/c2tx20016c.

SUPPLEMENTARY DATA

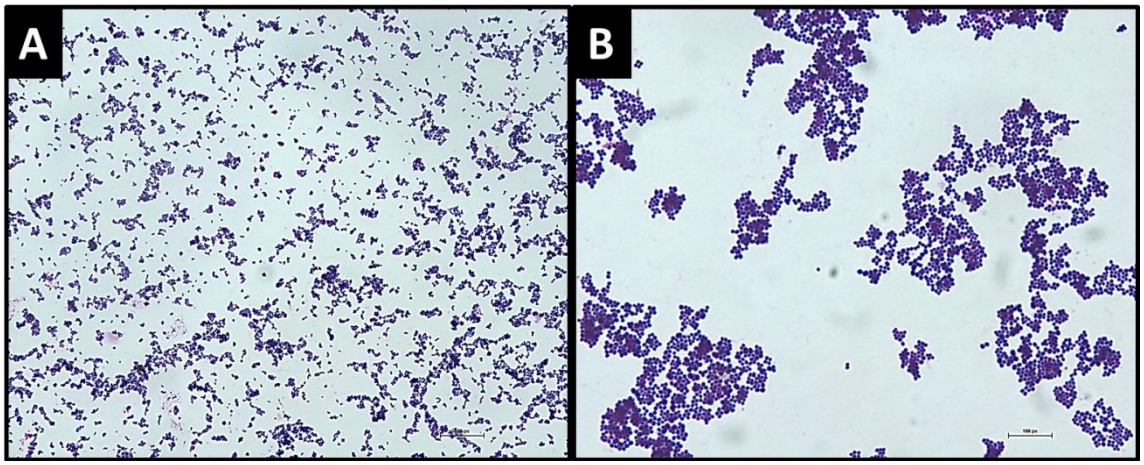

Supplementary Figure 1. Microscopic image of *R. mucilaginosa*(ATCC 66034) taken using bright field microscopy under 40x (A) and 100x(B) magnifications.

Yuh-Fen, Pung,etal. "Potent antifungal activity of ZnO Nanoparticles on *R.mucilaginosa* is mediated by reactive oxygen species and zinc ion." *IOSR Journal of Engineering (IOSRJEN)*, 10(4), 2020, pp. 44-57.